

Solar Wind Charge Exchange Contributions to the Diffuse X-Ray Emission

T. E. Cravens^a, I. P. Robertson^a, S. Snowden^b, K. Kuntz^c, M. Collier^b
and M. Medvedev^a

^a*Dept. of Physics and Astronomy, Malott Hall, 1251 Wescoe Hall Dr., University of Kansas, Lawrence, KS 66045 USA*

^b*NASA Goddard Space Flight Center, Greenbelt, MD, 20771 USA*

^c*Dept. of Physics and Astronomy, Johns Hopkins University, 366 Bloomberg Center, 3400 N. Charles St., Baltimore, MD 21218 USA*

Abstract: Astrophysical x-ray emission is typically associated with hot collisional plasmas, such as the million degree gas residing in the solar corona or in supernova remnants. However, x-rays can also be produced in cooler gas by charge exchange collisions between highly-charged ions and neutral atoms or molecules. This mechanism produces soft x-ray emission plasma when the solar wind interacts with neutral gas in the solar system. Examples of such x-ray sources include comets, the terrestrial magnetosheath, and the heliosphere (where the solar wind interacts with incoming interstellar neutral gas). Heliospheric emission is thought to make a significant contribution to the observed soft x-ray background (SXRb). This emission needs to be better understood so that it can be distinguished from the SXRb emission associated with hot interstellar gas and the galactic halo.

Keywords: x-rays, charge exchange, local bubble, heliosphere, solar wind
PACS: 95.85 Nv; 96.60 Vg; 96.50 Ci; 96.50 Zc

INTRODUCTION

A key diagnostic tool for hot astrophysical plasmas is x-ray emission [e.g., 1]. Hot plasmas produce x-rays collisionally, both in the continuum from free-free and bound-free (e.g., electron-ion recombination) transitions and as line emission from highly ionized species (bound-bound transitions). Examples of this type of emission are the extreme ultraviolet (EUV) and soft x-ray emission from the solar corona with its temperature of about 10^6 K [2] and x-ray emission from the hot interstellar medium, including the hot local bubble [3].

Other x-ray sources are known to exist in the solar system. These other sources are much colder than the solar corona and the x-rays are mostly powered from external inputs (cf. Cravens [4, 5]). For example, x-rays are emitted from planetary atmospheres (e.g., the atmosphere of Venus) due to K-shell fluorescence associated with the absorption of solar x-rays [6, 7] or due to elastic scattering of solar x-rays (e.g., Jovian disk emission; [8]). In the former mechanism, a solar x-ray photon ionizes from the K-shell of an atom, which then de-excites by the emission of an x-ray photon or an Auger electron. For a review of cometary and planetary x-ray emission see review papers by Krasnopolsky et al. [9], Cravens [4, 5], Lisse et al. [10, 11], and Bhardwaj et al. [12].

Another important type of solar system x-ray emission is the solar wind charge exchange (SWCX) mechanism which was first recognized at comets, which are now known to be strong x-ray sources with x-ray luminosities of 1 GW for active comets [cf. 9, 10, 11]. The first cometary x-ray observations were made for comet Hyakutake in 1996 by ROSAT (i.e., the German x-ray observatory - Roentgen satellite) [13]. Cravens [14] proposed that this soft x-ray emission was due to charge exchange reactions between heavy solar wind ions and cometary neutrals. The heavy product ions are left in excited states and emit soft x-ray or EUV photons (see reviews by Cravens [4, 5]). X-ray emission from the solar wind charge exchange (SWCX) mechanism shows up as numerous spectral lines [15, 16].

The SWCX mechanism should operate to produce x-rays wherever highly charged solar wind ions encounter neutral atoms and molecules [14]. Some x-ray emission from the solar wind interaction with neutrals in the exospheres of Venus, Mars, and Earth has been attributed to the SWCX mechanism [17, 18, 19, 6, 20]. Robertson and Cravens [19] used the SWCX mechanism applied to geocoronal hydrogen to generate simulated x-ray images of the magnetosheath plasma, and Robertson et al. [21] simulated the geocoronal x-ray emission expected during a geomagnetic storm and included the cusp regions. X-ray emission has also been observed from planets, from interstellar gas throughout the heliosphere, and from the Moon [cf. 22, 23, 24, 4, 5, 25]. The heliosphere is that region of space controlled by the outflowing solar wind plasma [26].

X-ray emission is produced via the SWCX mechanism as the solar wind interacts with the interstellar neutrals permeating our heliosphere [27, 4, 5, 18, 28, 29]. Why is this x-ray emission within the solar system relevant to the subject of the local hot bubble (LHB)? Soft x-ray emission has been used to study the properties of the hot interstellar medium (ISM), the LHB, and the ISM further away, such as the galactic halo [30, 27]. The x-ray spectrum produced from hot interstellar gas is quite similar to the SWCX spectrum. Figure 1 is a schematic of a line of sight of an x-ray observation passing through the terrestrial magnetosheath (and geocorona), the heliosphere, the LHB, and the galactic halo. Given the spectral similarity and the spatial diffusivity of the x-ray emission from all these regions, extracting information on the LHB alone from the total x-ray emission is not easy. In this chapter, we will review the SWCX mechanism and its possible contribution to the soft x-ray background (SXRb).

THE SOLAR WIND CHARGE EXCHANGE MECHANISM

The solar wind originates in the million degree solar corona. The coronal gas is collisionally ionized but becomes increasingly dilute (and eventually collisionless) as it flows out into the solar system becoming the solar wind. The corona is a powerful x-ray source with active regions of the Sun being hotter (i.e., $T \approx 2 \times 10^6$ K) and brighter in x-rays and quiet regions being cooler and dimmer ($T \approx 10^6$ K). The active regions are associated with closed loops of magnetic field. The composition of the solar corona (and the solar wind) is “solar” -- 92% hydrogen by volume, 8% helium, and 0.1% heavier elements which exist in high charge states (e.g., O^{7+} , C^{6+} , Fe^{12+} , ...). The ion composition and charge state distribution in the solar wind are “frozen-in” at coronal values due to rapidly decreasing collision frequency [31]. The solar wind is very structured, spatially

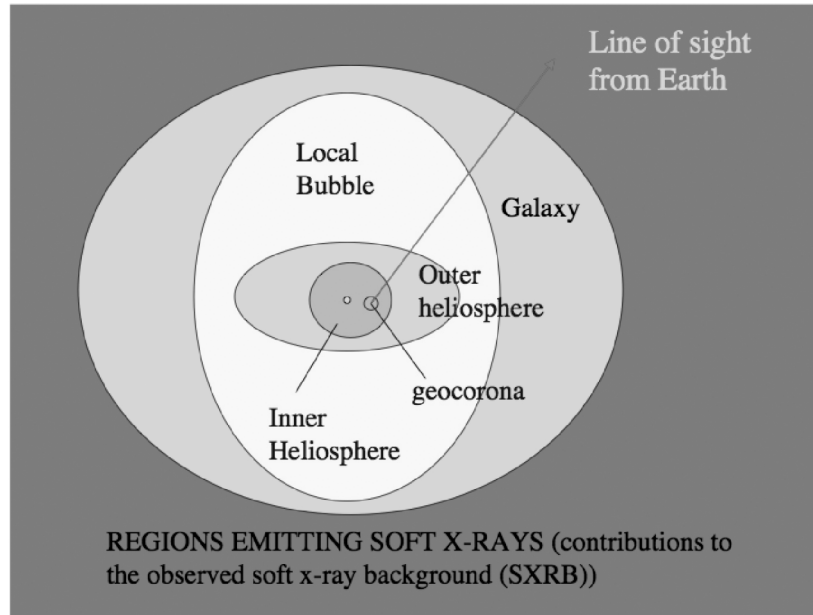


FIGURE 1. Schematic of an observational line of sight through the terrestrial geocorona, the inner and outer heliosphere, the local hot bubble, and the galaxy as a whole. Soft x-ray emission from each of these regions will contribute to the observed intensity.

and temporally, and contains slow (400 km/s) and fast (700 km/s) streams. The solar wind eventually “collides” with the ionized portion of the local interstellar medium at the heliopause, located about 150 AU from the Sun [26].

Highly charged, heavy solar wind ions (e.g., O^{6+} , O^{7+} , C^{6+} , Fe^{12+}) undergo charge transfer collisions with neutrals yielding excited product ions that emit photons. One such charge exchange (CX) reaction is:



M denotes a neutral target such as H or He. The product ion, O^{6+*} , starts out in a highly excited state [cf. 14, 4, 32, 33, 34, 35, 9] and x-ray and EUV photons are emitted as the ion de-excites.

Cross sections for charge exchange (CX) collisions for reactions such as (1) are very large [cf. 9, 34, 36]. Figure 2 shows some experimentally measured cross sections for several ion species colliding with water molecules at collision energies appropriate for solar wind conditions. The O^{7+} cross section is $\sigma \approx 5 \times 10^{-15} \text{ cm}^2$, much larger than the geometrical cross section. Over-the-barrier model (OBM) cross sections are also shown, as are the predicted principle quantum numbers of the product ions. For the excited product ion in equation (1), $n = 5$ is predicted, which is in agreement with the average value from more accurate scattering calculations. The main transitions for O^{6+} from reaction (1) are (in the x-ray spectrum) at photon energies of 574 eV, 568 eV, and 561 eV ($n=2$ to $n=1$), as well as from 653 eV and 750 eV lines associated with higher-lying states [28].

The x-ray volume emission rate (P_{sj}) at some location, \mathbf{r} , due to the SWCX mechanism for a given transition (j), is given by the product of the flux (Φ_{sq}) of the relevant solar wind ion species (s) and charge state (q), the relevant CX cross section (σ_{sq}), the density of neutral targets at \mathbf{r} (n_n), and the spectral cascading probability (b_{sqj}):

$$P_{sj}(\mathbf{r}) = \Phi_{sq} \sigma_{sq} b_{sqj} n_n(\mathbf{r}) \quad (2)$$

The x-ray intensity for a spectral line with energy, E_{sj} , is given by the integral over a relevant “optical” pathlength of the volume emission rate given by equation (2). Heavy ion abundances and charge state distributions in the solar wind vary both in time and space, with slow and fast-speed streams in particular having different charge state composition [cf. 37].

Most x-ray observations in the past have had rather poor spectral resolution. Broad-band x-ray power emission rates (and efficiencies) can be calculated by multiplying equation (2) with the energy E_{sj} and then adding the individual contributions over all transitions (over some x-ray and EUV energy interval) and adding over all solar wind species and charge states. It is often useful to express the flux of solar species/charge state ions as $\Phi_{sq} = f_{sq} n_{sw} u_{sw}$, where n_{sw} and u_{sw} are the solar wind proton density and speed, respectively, and f_{sq} is the fraction of species (s and q) in the solar wind. This approximation is useful because the proton flux ($n_{sw} u_{sw}$) exhibits more variability than the heavy ion abundances do (f_{sq}). The broad-band approach was taken in many studies [e.g., 14, 38, 18, 19] and is particularly useful for model comparisons with low spectral resolution data. Models making detailed spectral predictions [e.g., 39] need to preserve more details in equation (2). The predicted spectra need to be convolved with the appropriate instrumental response functions before being compared with observations (e.g., see the Robertson et al. chapter in this volume). X-ray spectra and emission efficiencies from the SWCX mechanism do not strongly depend on the neutral gas with which the solar wind interacts.

As mentioned earlier, comets are excellent sources of soft x-rays [cf. 4, 5, 9]. The nucleus of a comet is generally a few kilometers in diameter and contains a mixture of ice and dust. As the nucleus enters the inner solar system, water vapor sublimates from the ice, and, unimpeded by gravity, expands into space creating a large (10^5 km) gaseous and dust-filled coma. The extensive cloud of water, and its dissociation products (OH, O, H), act as targets for the solar wind. The x-ray emitting regions of active comets extend almost out to a million kilometers (see reviews by Lisse et al. [11]; Krasnopolsky et al. [9]; and Cravens [4]).

The SWCX-produced spectra for any object (e.g. comets, the geocorona, the heliosphere) are similar, particularly for similar solar wind types. The XMM Newton spectrum measured for comet LINEAR (C/1000 WM1) by Dennerl et al. [16]) provides a particularly good example (Figure 3). Some key spectral features are evident in this figure. Lines from O^{7+} and O^{6+} are found near photon energies of 650 eV (produced by CX of O^{7+} and O^{6+} , respectively), and lines near 565 eV due to the $n=2$ to $n=1$ transitions of O^{6+} (from CX of O^{7+}) are especially prominent. Carbon lines (both C^{5+} and C^{4+} lines - due to CX of C^{6+} and C^{5+} , respectively) dominate the 350 - 460 eV part of the spectrum. Below about 330 eV, the spectrum contains very large numbers of unresolved lines from metals (Mg, Fe, Si.....).

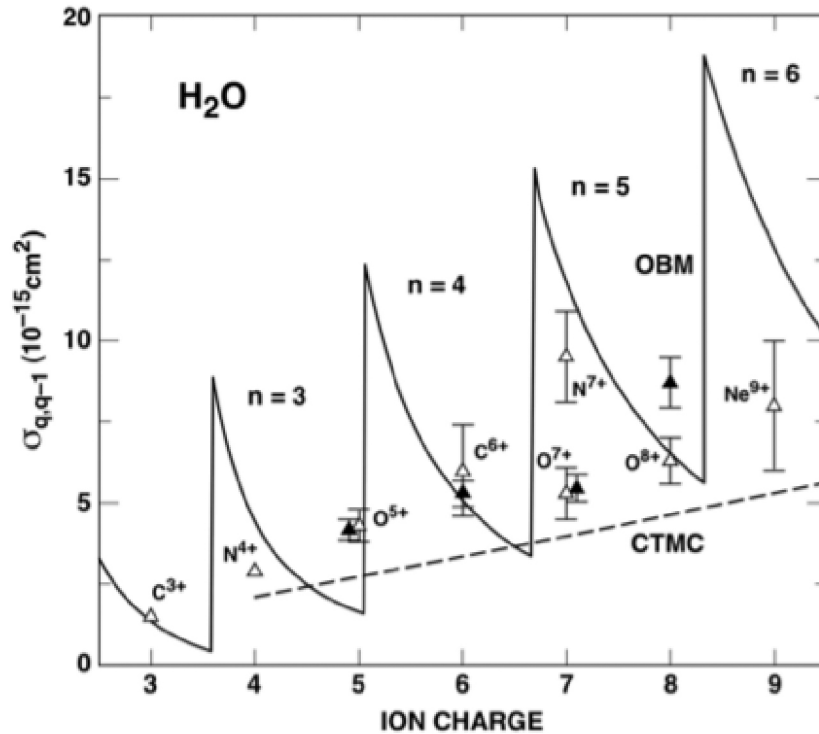


FIGURE 2. Cross sections for charge exchange of the ion species shown versus charge state. The data points are experimental measurements for collision energies appropriate for the solar wind (roughly 1 keV/amu). Simple theoretical classic over-barrier model (OBM) cross sections are shown, together with the principle quantum number predicted for the product ions. Some classical trajectory Monte Carlo (CTMC) theoretical results are also shown. Reprinted with permission from R. M. Mawhorter, A. R. Chutjian, T. E. Cravens, N. Djuric, S. Hossain, C. M. Lisse, J. MacAskill, S. J. Smith, and I. D. Williams, *Phys. Rev. A*, **75**, 032704 (2007). Copyright 2007 by the American Physical Society..

X-RAY EMISSION FROM THE TERRESTRIAL GEOCORONA AND MAGNETOSHEATH

X-rays are produced throughout the terrestrial magnetosheath as a consequence of charge transfer collisions between heavy solar wind ions and exospheric neutrals residing in the geocorona. The magnetosheath contains shocked solar wind downstream of the bow shock and outside the magnetopause, and the x-ray volume emission rate is particularly high in the subsolar part of this region due to the enhanced solar wind density. The neutral species for this SWCX x-ray source is atomic hydrogen residing in the geocorona. The expression adopted by Cravens et al. [41] in their x-ray model for the H-density was $n_H = n_{H0}(10R_E/r)^3$ (with $n_{H0} = 25 \text{ cm}^{-3}$), and was designed to approximate the Hodges [42] density profiles in the vicinity of the magnetopause (near $10 R_E$).

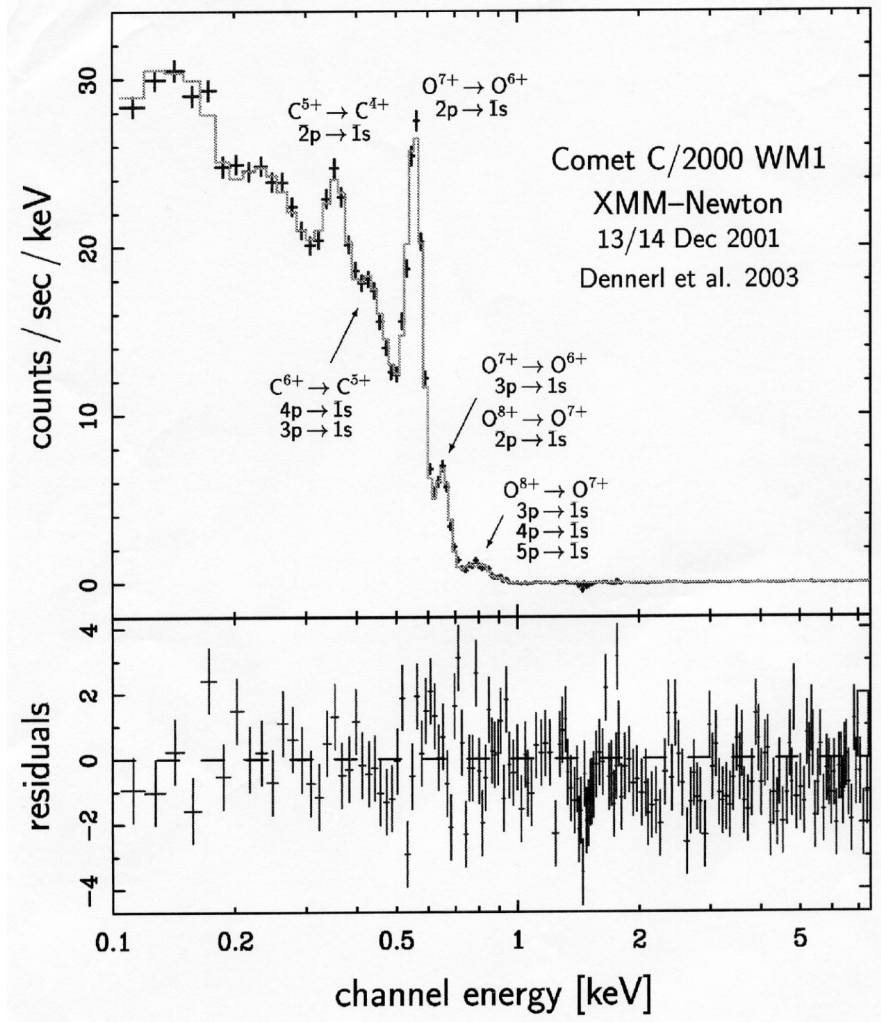


FIGURE 3. XMM Newton spectrum of comet LINEAR (C/2000 WM1). Photon count rate versus energy. From [16]; copyright 2003 SPIE.

As discussed in the introduction, the geocoronal x-ray emission was expected to be highly time variable due to the solar wind variations. This was verified (see Fig. 4 and [41]) by the correlation between the solar wind proton flux measured by the IMP-8 spacecraft and the time varying part of the diffuse soft x-ray flux (i.e., the so-called long term enhancements, or LTEs, measured in the $\frac{1}{4}$ keV ROSAT channel [43, 44]. Variations of SWCX-produced x-rays were also seen at comets and were attributed to: (1) temporal variations in the solar wind proton flux [45, 23, 24] and (2) variations in the relative solar wind heavy ion composition [45, 37]. The first source of variability appears to be dominant at least at shorter time-scales as demonstrated by correlations between the solar wind proton flux and x-ray emission at comets [45] and at Earth [41, 19].

A number of models of the geocoronal x-ray emission were constructed [46, 41, 19, 21]. The Robertson and Cravens model [19] predicted what an image in soft x-rays of the magnetosheath would look like, and this model used published terrestrial exospheric hydrogen densities [42] and used solar wind speeds, solar wind densities and temperature distributions in the magnetosheath from a numerical hydrodynamic model [47]. The

locations of the bow shock and the magnetopause were quite evident in the simulated images, thus suggesting that SWCX-produced x-rays could be used as a tool for studying solar-terrestrial physics.

Robertson et al. [21] constructed an even more sophisticated geocoronal x-ray model using dynamic three-dimensional MHD simulations of the solar wind, magnetosheath and magnetosphere for the March 31st, 2001, geomagnetic storm. A sky map of simulated x-ray emission was generated as would be seen by a hypothetical x-ray detector on the IMAGE spacecraft. Figure 5 is a simulated image taken from an observation point well outside the geocorona and in which the cusps can clearly be detected.

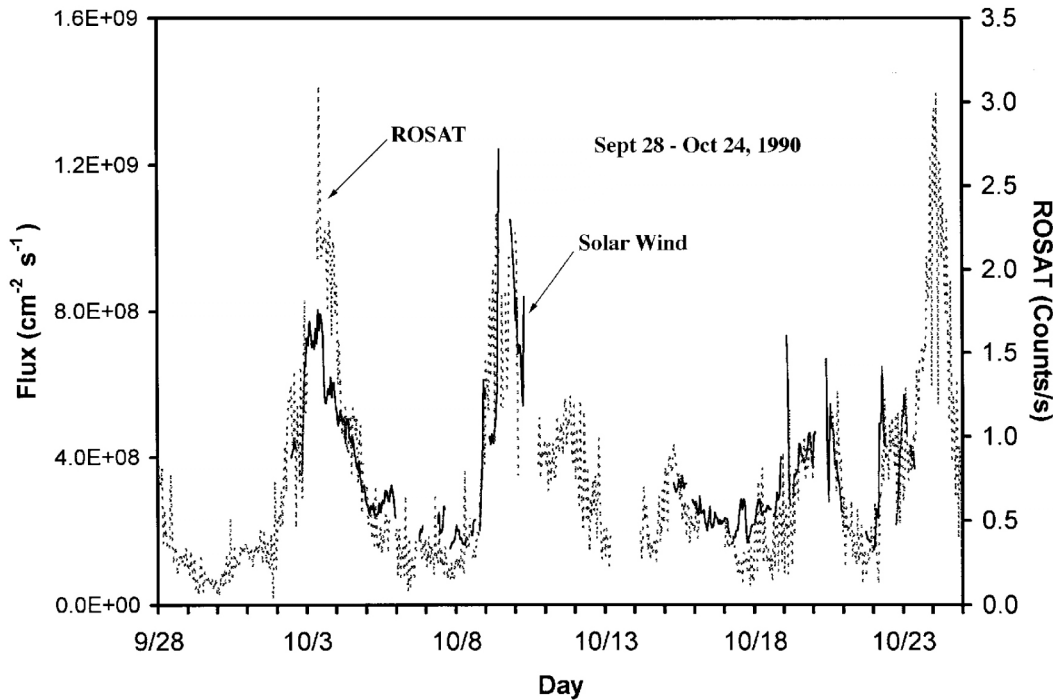


FIGURE 4. Soft x-ray flux (ROSAT ¼ keV channel count rate) (right scale) and solar wind proton flux measured near Earth (left scale) versus time (units of days). From [41]; copyright 2001 American Geophysical Union--further reproduction or electronic distribution is not permitted.

X-RAY EMISSION FROM THE HELIOSPHERE

The region of space containing solar wind plasma (and solar magnetic field) is called the heliosphere. The boundary between the heliosphere and the local interstellar medium is called the heliopause [cf. 26, 48, 49, 50]. The solar wind flow undergoes a shock, called the termination shock, before it reaches the heliopause, and both Voyager spacecraft have just recently crossed this shock at distances of ≈ 95 AU [51]. Neutral atoms from the local interstellar cloud surrounding the heliosphere “freely” enter our solar system with a speed of about 23 km/s [52, 53], but the interstellar plasma and magnetic field are kept out of the heliosphere by the outflowing solar wind. The ionized component of the very local interstellar medium (VLISM) cannot enter the heliosphere

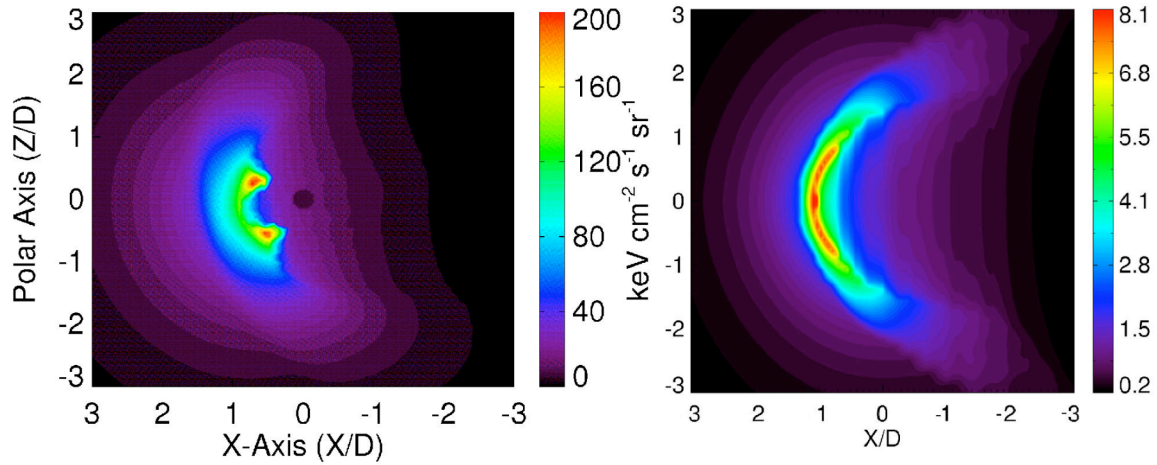


FIGURE 5. Simulated x-ray intensities for the terrestrial magnetosheath for the March 31st, 2001, arrival at Earth of a solar event, as observed from the GSM y-axis 50 R_E removed from Earth (left). Units are in D – distance to the subsolar magnetopause. The right side is an x-ray image for average solar wind conditions [19]. Note that the color scales for intensity are very different. From [21]; copyright 2001 American Geophysical Union--further reproduction or electronic distribution is not permitted.

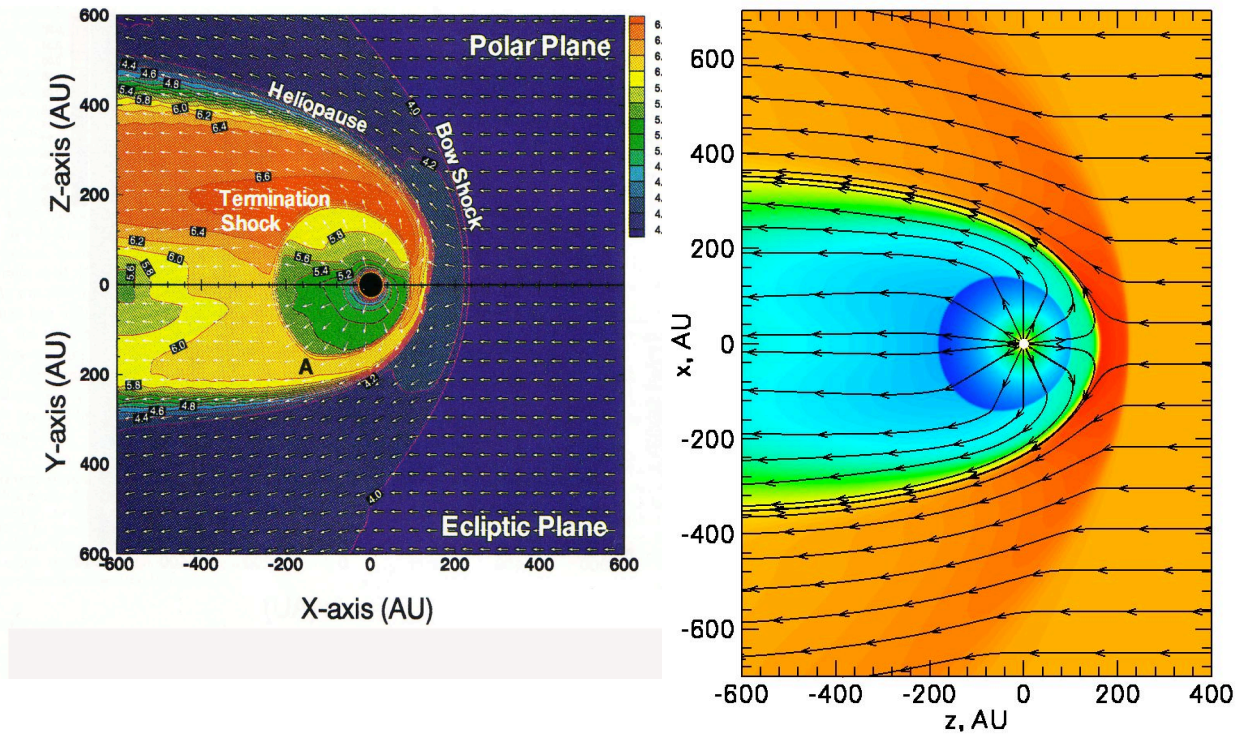


FIGURE 6. (left) Proton temperature (actually log-10 of temp.) contours and plasma flow vectors in the polar plane and in the ecliptic plane of our heliosphere from the model of Pauls and Zank [48]. Key regions of the solar wind – local interstellar medium interaction are indicated. (right) Illustration of stream lines in the outer heliosphere.

and has not been directly measured, although indirectly it has been inferred that the plasma density is about $\approx .01 \text{ cm}^{-3}$. The very local interstellar cloud is about 1 – 2 pc across [54] but this cloud (and many others) is immersed in a hot ionized gas region called the “local hot bubble” (LHB) which is observed using soft x-rays [44, 55]. Figure 6 shows some results from the dynamical model of Zank and Pauls [50]. The dynamical boundaries just mentioned and plasma streamlines are evident in this figure.

Atomic hydrogen and atomic helium are the main neutral interstellar neutral species [56, 57]. The density of interstellar hydrogen is about 0.15 cm^{-3} and the density of helium is about 10% that of the hydrogen. The inflowing hydrogen interacts weakly with the plasma via charge transfer reactions near the heliopause [52], creating a “hydrogen wall” in which the H density is somewhat enhanced. In the inner heliosphere within a few AU, interstellar hydrogen is affected by solar radiation pressure and the gravitational force of the Sun, creating a cavity in the H distribution around the Sun. The H density is greater upwind than it is downwind. Interstellar helium does not interact with solar wind plasma and radiation pressure is not very effective, so that interstellar helium can be found closer to the Sun than interstellar hydrogen. But gravitational focusing creates a high-density helium “focusing” cone in the downwind direction at heliocentric distances of 1-2 AU [57].

X-rays due to the interaction of the solar wind with interstellar neutrals are emitted from the entire heliosphere, as first recognized by Cox [27]. Cravens [46] constructed a simple model of heliospheric x-ray emission from charge exchange between the solar wind and interstellar helium and hydrogen and demonstrated that the intensities were significant and that the spectral shape was consistent with that of the observed soft x-ray background emission [30]. Cravens [46] noted that the emission observed from Earth is dominated by the inner heliosphere (heliocentric distances within $\approx 10 \text{ AU}$) and it is this region that contributes to the diffuse SXR. Cravens et al. [41] and Robertson et al. [38] developed a simple time-dependent model of the soft x-ray emission from the SWCX mechanism applied to both the interstellar neutrals (both H and He) and geocoronal hydrogen.

The outer heliosphere contributes a major part of the total x-ray luminosity (as would be observed from the outside), but its contribution to Earth-based intensities is only $\approx 25\%$ [18, 58], with most of this emission originating from the shocked solar wind gas in the heliosheath (and hydrogen wall) located between the termination shock and the heliopause. Figure 7 shows a simulation of what heliospheric x-ray emission from O^{6+} lines (due to CX of solar wind O^{7+}) would look like from the outside [58]. Medvedev et al. also constructed full x-ray spectra for viewing direction towards the nose and tail of the heliosphere (not shown here), demonstrating that the latter exhibited the effects of collisional thickness for CX collisions. Wargelin and Drake [59] looked for the analogous CX x-ray emission from the “astrosphere” of the nearby star Proxima Centauri and were only able to set an upper limit on such emission.

The heliospheric emission observed from Earth and its potential contribution to the SXR has been extensively studied over the past 10 years [e.g., 27, 46, 38, 28, 60, 29, and Robertson et al. in this book]. X-ray emissions associated with interstellar helium and hydrogen have different directional spatial distributions and also have different temporal responses to solar wind variations. The helium-based x-ray emission shows enhancement in the downwind direction (due to the focusing cone) and responds

relatively quickly to solar wind variations, although not as quickly as geocoronal x-ray emission does. Due to the travel time of the solar wind to different regions of the heliosphere [41, 18] and due to corotating solar wind structures [29, 61], the time history of the helium-based x-ray emission can be quite complex. Hydrogen-based x-ray emission originates from larger heliocentric distances and is most intense in the upwind direction, and it exhibits very little temporal variation due to the large volume it is produced from.

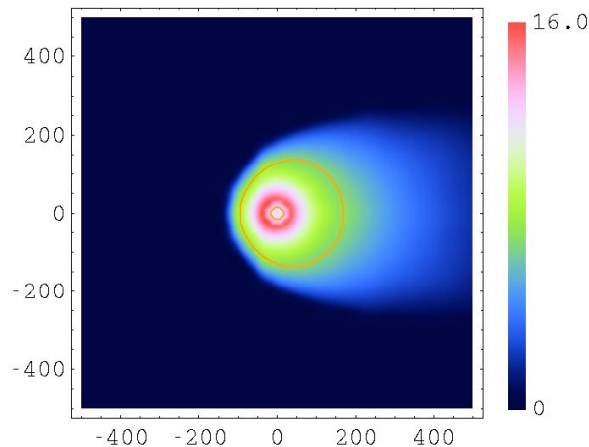


FIGURE 7. Image of heliospheric x-ray emission in O^{6+} lines (from solar wind O^{7+} charge exchange), as viewed from outside. An intensity scale is shown. The coordinate units are astronomical units and the interstellar flow is from the left. The red line is the estimated position of the termination shock (as viewed from the limb). Reprinted with permission from M. V. Medvedev, I. P. Robertson, T. E. Cravens, G. P. Zank, and V. Florinski, Charge exchange X-rays from the heliosheath, in *Physics of the Inner Heliosheath: Voyager Observations, Theory, and Future Prospects*, AIP Conference Proc., **858**, 348 (2006). Copyright 2006, American Institute of Physics.

Figure 8 shows calculated time histories of the x-ray emission from the geocorona, heliospheric H, and heliospheric He for a particular look direction and using measured solar wind fluxes versus time [41, 19]. The relative contributions and time dependences of the x-ray emission depend on the look direction. The “baseline” x-ray intensity is what matters for the problem of evaluating the local contribution to the SXRb and deducing the properties of the hot interstellar medium, including the LHB. In the past, observers have removed the time-varying x-ray emission (such as LTEs) from the SXRb to the extent they could [e.g., 44, 55], but the steady heliospheric H-contribution is difficult to distinguish. Time averaged intensities have been found from intensity calculations such as those shown in Fig. 8 by a number of authors (using somewhat different methods) and as a function of look direction.

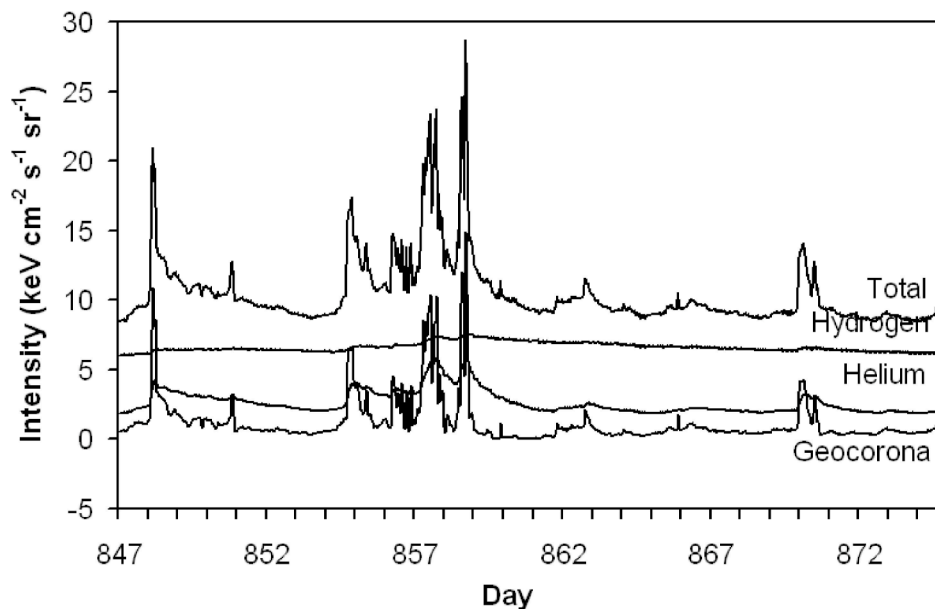


FIGURE 8. Time history of SWCX produced x-ray emission intensities as observed from Earth calculated for an upwind look direction and during fall equinox. Contributions from the geocorona and from heliospheric H and He are shown. From [19]; copyright 2001 American Geophysical Union--further reproduction or electronic distribution is not permitted.

Robertson and Cravens [18] used an average steady solar wind flux and included the geocoronal and heliospheric emission components to create sky maps of the local soft x-ray intensity in order to compare with the ROSAT $\frac{1}{4}$ keV channel sky maps used in deducing properties of the LHB [55]. The conversion between model x-ray intensity and ROSAT $\frac{1}{4}$ keV count rate was determined by comparing (from other ROSAT observations) the measured LTE time variations with model variations. This allowed Robertson and Cravens to “normalize” their map. They concluded that at low galactic latitudes about 50% of the observed $\frac{1}{4}$ keV emission could be explained by the heliospheric emission. The heliosphere evidently did not make much of a contribution to the more intense emission observed at high-latitudes (which also includes galactic halo contributions [62]). Lallement [60] used a scaling factor to determine the maximum heliospheric contribution to the sky map and concluded that there is considerably less hot gas emission in the local bubble than previously thought (i.e., almost no LHB emission at some galactic longitudes), thus reducing the pressure discrepancy between the local bubble and our heliosphere by a factor of 4.

Koutroumpa et al. [61, 29] focused on SWCX-produced heliospheric x-ray emission in the 0.57 keV (OVII triplet) and 0.65 keV (OVIII) lines and made detailed comparisons of a model with XMM-Newton, Chandra, and Suzaku data in certain look directions. They concluded that all of the $\frac{3}{4}$ keV channel ROSAT SWRB emission could be explained by local emission, which puts severe constraints on the temperature of the local bubble gas. Robertson et al. (2009 -- chapter in this volume) redid the Robertson et al. [18] study by using the appropriate time-dependent solar wind in the model and then taking “baseline” intensities, rather than just using a steady solar wind. This procedure more accurately mimics the Snowden et al. [43] data-handling procedures. The new

model also generates both $\frac{1}{4}$ keV and $\frac{3}{4}$ keV channel simulated ROSAT count rates by feeding SWCX spectra into the appropriate ROSAT response matrices. They conclude again that about 50% of the low latitude $\frac{1}{4}$ keV emission is local (and not LHB) and they also conclude that about 50% of the low latitude $\frac{3}{4}$ keV emission is heliospheric (and not LHB).

DISCUSSION AND SUMMARY

Work done over the past ten years on heliospheric x-ray emission has shown that this local emission can account for at least half of the soft x-ray background emission at low galactic latitudes for $\approx \frac{1}{4}$ keV x-rays and perhaps even more of the $\frac{3}{4}$ keV emission. The dynamics and structure of the local hot bubble, as envisioned in the previous 1998 volume, must be altered accordingly. One consequence is that the thermal pressure of the hot gas should be less than previously thought ($P_{\text{th}}/K \sim 11,000 \text{ K cm}^{-3}$ as opposed to $15,000 \text{ K cm}^{-3}$), which actually helps the pressure balance between the LHB and the very local cloud [60, 62]. Other chapters in this volume explore some of these issues.

However, our current estimates of the local contributions to the SXR background reviewed here still remain quite uncertain. Local and cosmic x-ray emission can potentially be distinguished by: (1) using time variability of some local emission (e.g., geocoronal emission - LTEs), (2) using the spatial variations (upwind-downwind) plus detailed modeling (the main method used to account for the heliospheric emission), and (3) using details of the spectrum.

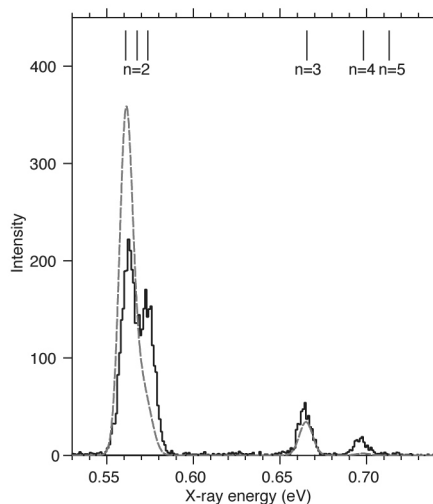


FIGURE 9. A spectrum measured in the laboratory with a microcalorimeter. Emission from O^{6+} is produced by charge exchange between O^{7+} ions and CO_2 . The dashed line shows a prediction strongly favoring the forbidden line. From P. Beiersdorfer et al., *Science*, **300**, 1558, 2003; reprinted with permission from AAAS.

Differences between the spectral characteristics of SWCX-produced x-rays and x-rays from the hot LHB gas have not yet been exploited for a couple of reasons: (1) spectral differences between SWCX-produced x-rays [e.g., 28] and hot gas collisional x-

rays [e.g., 64, 1] are not fully understood (both types of emission have similar species and transitions present - the differences are in the details), and (2) the spectral resolution of current SXR observations is low (at the CCD level - 60 eV or worse) with a couple of exceptions. Sanders et al. [65] flew a Bragg-crystal spectrometer onboard the space shuttle and made high spectral resolution measurements for a small part of the sky in the 148 – 284 eV energy range.

A systematic set of high-resolution (e.g., microcalorimeter) observations needs to be carried out over a far wider range of photon energies and for extensive sky coverage. Microcalorimeters could provide high spectral resolution ($\Delta E \approx 10$ eV), as shown from the laboratory spectrum reproduced in Fig. 9. Beiersdorfer et al. [63] note that the spectrum of helium-like O^{6+} is dominated by emission from the forbidden transition $1s2s\ ^3S_1 - 1s^2\ ^1S_0$, whereas collisional excitation produces much more emission from the resonance line $1s2p\ ^1P_1 - 1s^2\ ^1S_0$. With a systematic set of such high-resolution observations covering a large part of the sky, spectral differences could be exploited to distinguish between local SWCX emission and more distant collisional emission associated with the hot gas in the interstellar medium.

ACKNOWLEDGMENTS

This material is based upon work supported by the National Aeronautics and Space Administration under Grant No. NNH06ZDA001N-ADP issued through the Science Mission Directorate's Astrophysics Division.

REFERENCES

1. D. F. Cioffi, "Supernova remnants as probes of the interstellar medium" in *Physical Processes in Hot Cosmic Plasma*, edited by W. Brinkmann, A. C. Fabian, and F. Giovannelli, p. 1, Kluwer, Dordrecht, The Netherlands, 1990.
2. H. Zirin, *Astrophysics of the Sun*, Cambridge and New York, Cambridge University Press, 1988.
3. K. D. Kuntz and S. L. Snowden, *Astrophys. J.*, **543**, 195 (2000).
4. T. E. Cravens, *Science*, **296**, 1042 (2002a).
5. T. E. Cravens, AIP Conference Proceedings, **635**(1), 173 (2002b).
6. K. Dennerl, V. Burwitz, J. Englhauser, C. Lisse, and S. Wolk, *Astron. Astrophys.*, **386**, 319 (2002).
7. T. E. Cravens, and A. N. Maurellis, *Geophys. Res. Lett.*, **28**(15), 3043 (2001).
8. A. N. Maurellis, T. E. Cravens, G. R. Gladstone, J. H. Waite, and L. W. Acton, *Geophys. Res. Lett.*, **27**(9), 1339 (2000).
9. V. A. Krasnopolsky, J. B. Greenwood, and P. C. Stancil, *Space Sci. Rev.*, **113**, 271 (2005).
10. C. M. Lisse, D. J. Christian, K. Dennerl, S. J. Wolk, D. Bodewits, R. Hoekstra, M. R. Combi, T. Mäkinen, M. Dryer, C. D. Fry, and H. Weaver, *Astrophys. J.*, **635** 1329 (2005a).
11. C. M. Lisse, T. E. Cravens, and K. Dennerl, X-ray and extreme ultraviolet emission from comets, in *Comets II*, edited by M. Festou, H. Keller, and H. A. Weaver, pp. 631-646, Univ. of Arizona Press, Tucson (2005b).
12. A. Bhardwaj et al., Soft x-ray emissions from planets, moons, and comets, in *Earth-like Planets and Moons*, Proc. 36th ESLAB Symposium, ESA SP-514, edited by B. Foing, and B. Battrick, pp. 215 – 226, ESTEC, Noordwijk, The Netherlands (2002).
13. C. M. Lisse, K. Dennerl, J. Englhauser, M. Harden, F. E. Marshall, M. J. Mumma, R. Petre, J. P. Pye, M. J. Ricketts, J. Schmitt, J. Trümper, and R.G. West, *Science*, **274**, 205 (1996).
14. T. E. Cravens, *Geophys. Res. Lett.*, **24**, 105 (1997).

15. C. M. Lisse, D. J. Christian, K. Dennerl, K. J. Meech, R. Petre, H. A. Weaver, and S. J. Wolk, *Science*, **292**, 1343 (2001).
16. K. Dennerl, B. Aschenbach, V. Burwitz, J. Englhauser, C. M. Lisse, and P. M. Rodriguez-Pascual, A major step in understanding the x-ray generation in comets: Recent progress obtained with XMM-Newton, in *X-Ray and Gamma-Ray Telescopes and Instruments for Astronomy*, Proc. SPIE, **4851**, 277 (2003).
17. M. Holmström, S. Barabash, and E. Kallio, *Geophys. Res. Lett.*, **28**(7), 1287 (2001).
18. I. P. Robertson and T. E. Cravens, *J. Geophys. Res.*, **108**, A10, 8031, doi:10.1029/2003JA009873 (2003a).
19. I. P. Robertson and T. E. Cravens, *Geophys. Res. Lett.*, **30**(8), 1439, doi:10.1029/2002GL016740 (2003b).
20. K. Dennerl, *Astron. Astrophys.*, **394**, 1119 (2002).
21. I. P. Robertson, M. R. Collier, T. E. Cravens, and M.-C. Fok, *J. Geophys. Res.*, **111**, A12 (2006).
22. K. Dennerl, J. Englhauser, and J. Trümper, *Science*, **277**, 1625 (1997).
23. C. M. Lisse, K. Dennerl, J. Englhauser, J. Trümper, F. E. Marshall, R. Petre, A. Valina, B. J. Kellett, and R. Bingham, *Earth Moon Planets*, **77**, 283 (1999a).
24. C. M. Lisse et al., *Icarus*, **141**, 316 (1999b).
25. A. Bhardwaj, et al., *Planet. Space Sci.*, **55**, 1135 (2007).
26. S. T. Suess, *Reviews of Geophysics*, **28**, 97 (1990).
27. D. P. Cox, Modeling the local bubble, in *The Local Bubble and Beyond*, edited by D. Breitschwerdt, M. J. Freyberg, and J. Trümper, p. 121, Springer, Berlin (1998).
28. R. Pepino, R., V. Kharchenko, and A. Dalgarno, *Astrophys. J.*, **617**, 1347 (2004).
29. D. Koutroumpa, D., F. Acero, R. Lallement, J. Ballet, and V. Kharchenko, *Astron. Astrophys.*, **475**, 901 (2007).
30. D. McCammon and W. T. Sanders, *Ann. Rev. Astron. Astrophys.*, **28**, 657 (1990).
31. A. J. Hundhausen, *Planet. Space Sci.*, **16**, 783 (1968).
32. R. M. Häberli, T. I. Gombosi, D. L. De Zeeuw, M. R. Combi, and K. G. Powell, *Science*, **276**, 939 (1997).
33. R. Wegmann, H. U. Schmidt, C. M. Lisse, K. Dennerl, and J. Englhauser, *Planet. Space Sci.*, **46**, 603 (1998).
34. J. B. Greenwood, I. D. Williams, S. J. Smith, and A. Chutjian, *Astrophys. J.*, **533**, L175 (2000).
35. V. Kharchenko and A. Dalgarno, *J. Geophys. Res.*, **105**, 18,351 (2000).
36. R. M. Mawhorter, N. Djuric, S. Hossain, J. Macaskill, S. J. Smith, and A. Chutjian, Absolute charge exchange cross sections for $C^{3,4,5,6+}$, $N^{4,5+}$, $O^{5,6,7+}$, and $Ne^{7,8+}$ collisions with H_2O , CH_4 , CO , and CO_2 , American Physical Society, 37th Meeting of the Division of Atomic, Molecular and Optical Physics, May 16-20, 2006.
37. N. A. Schwadron and T. E. Cravens, *Astrophys. J.*, **544**, 558 (2000).
38. I. P. Robertson, T. E. Cravens, S. L. Snowden, and T. Linde, Temporal and spatial variations of heliospheric x-ray emissions associated with charge transfer of the solar wind with interstellar neutrals, in *The 3-D Heliosphere at Solar Maximum*, Proc. of the 34th ESLAB Symposium, edited by R. Marsden, p. 401, Springer, The Netherlands (2001).
39. V. Kharchenko and A. Dalgarno, *Astrophys. J.*, **554**, L99 (2001).
40. R. M. Mawhorter, A. R. Chutjian, T. E. Cravens, N. Djuric, S. Hossain, C. M. Lisse, J. MacAskill, S. J. Smith, and I. D. Williams, *Phys. Rev. A*, **75**, 032704 (2007).
41. T. E. Cravens, I. P. Robertson, and S. L. Snowden, *J. Geophys. Res.*, **106**, 24,883 (2001).
42. R. R. Hodges, Jr., *J. Geophys. Res.*, **99**, 23229 (1994).
43. S. L. Snowden, D. McCammon, D. N. Burrows, and J. A. Mendenhall, *Astrophys. J.*, **424**, 714 (1994).
44. S. L. Snowden, M. J. Freyberg, P. Plucinsky, J. H. M. M. Schmitt, J. Trümper, W. Voges, R. J. Edgar, D. McCammon, and W. T. Sanders, *Astrophys. J.*, **454**, 643 (1995).
45. M. Neugebauer, T. E. Cravens, C. M. Lisse, F. M. Ipavich, R. von Steiger, P. D. Shah, and T. P. Armstrong, *J. Geophys. Res.*, **105**, 20,949 (2000).
46. T. E. Cravens, *Astrophys. J.*, **532**, L153 (2000).
47. J. R. Spreiter, A. L. Summers, and A. Y. Alksne, *Planet. Space Sci.*, **14**, 223 (1966).
48. H. L. Pauls and G. P. Zank, Modeling of the solar wind/interstellar wind interaction, *Proc. 25th Int. Cosmic Ray Conf.* **2**, 241 (1997).

49. G. P. Zank, H.-R. Müller, V. Florinski, and P. C. Frisch, Solar journey: The significance of our galactic environment for the heliosphere and earth, in *Astrophysics and Space Science Library*, edited by Priscilla C. Frisch, Vol. 338. Springer, Dordrecht, 2006.
50. G. P. Zank and H. L. Pauls, *Space Sci. Rev.*, **78**, 95 (1996).
51. L. F. Burlaga, N. F. Ness, and M. H. Acuña, *Astrophys. J.*, **668**(2), 1246 (2007).
52. P. C. Frisch, The Local Bubble, Local Fluff, and Heliosphere, in *The Local Bubble and Beyond*, edited by D. Breitschwerdt, M. J. Freyberg, and J. Trümper, p. 269, Springer-Verlag, New York (1998).
53. H. J. Fahr, W. Neutsch, S. Grzedzielski, W. Macek, and R. Ratkiewicz-Landowska, *Space Sci. Rev.*, **43**, 329 (1986).
54. P. C. Frisch, *Space Sci. Rev.*, **72**, 499 (1995).
55. S. L. Snowden, R. Egger, M. J. Freyberg, D. McCammon, P. P. Plucinsky, W. T. Sanders, J. H. M. M. Schmitt, J. Truemper, and W. Voges, *Astrophys. J.*, **485**, 125 (1997).
56. E. Quémerais, R. Lallement, and J.-L. Bertaux, *J. Geophys. Res.*, **98**, 15,199 (1993).
57. E. Möbius, D. Rucinski, D. Hovestadt, and B. Kleckler, *Astron. Astrophys.*, **304**, 505 (1995).
58. M. V. Medvedev, I. P. Robertson, T. E. Cravens, G. P. Zank, and V. Florinski, Charge exchange X-rays from the heliosheath, in *Physics of the Inner Heliosheath: Voyager Observations, Theory, and Future Prospects*, AIP Conference Proc., 5th Annual IGPP International Astrophysics Conference, **858**, 348 (2006).
59. B. J. Wargelin and J. J. Drake, *Astrophys. J.*, **578**(1), 503 (2002).
60. Lallement, R., *Astron. Astrophys.*, **418**, 143, 2004.
61. D. Koutroumpa, R. Lallement, V. Kharchenko, A. Dalgarno, R. Pepino, V. Izmodenov, and E. Quémerais, *Astron. Astrophys.*, **460**, 289 (2006).
62. R. L. Shelton, *Space Sci. Rev.*, **143**, 231, doi: 10.1007/s11214-008-9358-8 (2008).
63. P. Beiersdorfer et al., *Science*, **300**, 1558 (2003).
64. R. Mewe, Ionization of hot plasmas, in *Physical Processes in Hot Cosmic Plasmas*, edited by W. Brinkman, A. C. Fabian, and F. Giovannelli, NATO, ASI series, Kluwer Academic Publishers, Dordrecht, p. 39 (1990).
65. W. T. Sanders, R. J. Edgar, W. L. Kraushaar, D. McCammon, and J. P. Morgenthaler, *Astrophys. J.*, **554**, 694 (2001).